Medium-Term Prediction of Chaos

Christopher C. Strelioff and Alfred W. Hübler

Center for Complex Systems Research, Department of Physics, University of Illinois at Urbana-Champaign, 1110 West Green Street, Urbana, Illinois 61801, USA

(Received 25 August 2005; published 30 January 2006)

We study prediction of chaotic time series when a perfect model is available but the initial condition is measured with uncertainty. A common approach for predicting future data given these circumstances is to apply the model despite the uncertainty. In systems with fold dynamics, we find prediction is improved over this strategy by recognizing this behavior. A systematic study of the Logistic map demonstrates prediction of the most likely trajectory can be extended three time steps. Finally, we discuss application of these ideas to the Rössler attractor.

DOI: 10.1103/PhysRevLett.96.044101 PACS numbers: 05.45.Tp, 05.45.Ac, 05.45.Pq

Development of methods for prediction and characterization of time series continues to be an active area of research [1–3]. In particular, methods developed for analyzing chaotic dynamics have an increasing number of applications. Some representative examples include prediction of epileptic seizures [4], analysis of population dynamics in ecology [5], prediction of equipment failure [6], and understanding error in weather prediction [7,8]. Much of the fundamental research on chaotic time series focuses on two general ideas. The first is inference of model parameters for prediction of future data [9–11]. In general this is effective for a short-term description of the system. The second approach focuses on estimation of average quantities or an invariant measure for classification of long-term behavior [12,13].

We propose an extension of these viewpoints by incorporating ideas from both short- and long-term approaches. We treat the initial condition as a measurement with uncertainty, resulting in an initial probability density function (PDF). While propagation of a probability density with underlying chaotic dynamics has been studied analytically [14,15], a direct connection to prediction of time series has not been made to our knowledge. Our goal is to use an understanding of PDF dynamics to identify the most probable trajectory.

We find prediction of a trajectory using these ideas to be very effective in systems with fold dynamics. Two well-known examples of chaotic systems with this behavior are the Logistic map [16] and Rössler attractor [17]. A perfect model, using an initial condition measured with uncertainty, will not accurately describe the most probable trajectory beyond the short term in these systems. The evolution of the initial PDF will develop new peak(s) due to the fold dynamics. These peaks are generally not related to images of the measured value and prediction of a trajectory begins to fail. Recognition of this effect is the key to extending prediction of a trajectory into the medium-term regime.

This Letter is organized as follows. First, we describe a general one-dimensional map and the properties necessary to produce fold dynamics. Next, we introduce a model of measurement with uncertainty which produces an initial PDF. We then consider evolution of an ensemble of trajectories consistent with this measurement. This material motivates the proposed prediction method and a systematic numerical study of our approach verifies its effectiveness. Finally, the extension of these ideas to higher dimensional systems is discussed. In particular, we discuss the application of the proposed method to coupled Logistic maps and the Rössler attractor.

As an illustration of our method, we focus on a 1-dimensional map

$$x_{n+1} = f(x_n, a). \tag{1}$$

To investigate fold dynamics we require $f(x, a)$ be differentiable on its domain with one or more critical points x_c^i, where $f'(x_c^i, a) = 0$ and $f''(x_c^i, a) \neq 0$. Given these properties, new peaks in the PDF will always be associated with images of the critical point(s). As an example of a map with these properties, we introduce the nonhyperbolic Logistic map $f(x, a) = ax(1 - x)$, where $a \in [0, 4]$ and $x \in [0, 1]$. For this map we have $f'(x_c, a) = 0$ at $x_c = 1/2$, and $f''(x_c, a) = -2a$.

The first step in prediction is specification of an initial condition. We propose the following model for measurement. The relationship between the true initial state x and the measured value m is given by $m = x + r$. The uncertainty in the measurement is reflected by r, with probability density $\rho(r)$. We will use the normal distribution with mean zero and small variance. This choice is designed to model random, nonsystematic uncertainty. The resulting form is a distribution consistent with the measured value and type of uncertainty assumed.

The range of possible trajectories which can be followed by an initial condition with uncertainty is investigated by constructing an ensemble. The first step is to generate a set of n_d initial conditions $\{x_j | j = 0, 1, \ldots, n_d - 1\}$, consistent with the type of measurement uncertainty assumed above. The time evolution of each x_j with Eq. (1) is used to produce the set of possible trajectories $\{f^{(n)}(x_j, a)\}$. We use the notation $f^{(n)}(x, a)$ to indicate n applications of the map to x.

A histogram is constructed from the ensemble to provide a coarse-grained approximation of the PDF $\rho_n(x)$. The region of interest is divided into n_b equally sized bins labeled $\mathcal{B}_i = [x_{\min} + iW_i, x_{\min} + (i+1)W_i)$, where $i = 0, 1, \ldots, n_b - 1$. The width of each bin is $W_i = (x_{\max} - x_{\min})/n_b$, where $x_{\min}$ and $x_{\max}$ are the minimum and maximum of $\{f^{(n)}(x_j, a)\}$ for all x_j and n. In this way, the bins cover the region of interest $\cup_i \mathcal{B}_i = [x_{\min}, x_{\max}]$. The complete histogram at time n is given by

$$H_n(x) = \sum_{i=0}^{n_b-1} H_{n,i} \mathbb{1}_{\mathcal{B}_i}(x), \tag{2}$$

where the estimated probability density for $\mathcal{B}_i$ at time n is

$$H_{n,i} = \frac{1}{n_d W_i} \sum_{j=0}^{n_d-1} \mathbb{1}_{\mathcal{B}_i}(f^{(n)}(x_j, a)). \tag{3}$$

In the above equations $\mathbb{1}_{\mathcal{B}_i}(x) = 1$ if $x \in \mathcal{B}_i$, and is zero otherwise. The value given in Eq. (3) is associated with the center of the bin $x_i = x_{\min} + (i + 1/2)W_i$. The path followed by the largest fraction of the ensemble identifies the most likely trajectory at each time step and is associated with the bin with largest probability density, $H_{n,i}$.

Figure 1 provides an illustration of typical dynamics for the Logistic map at $a = 3.80$, a value which produces chaotic dynamics. The ensemble of initial conditions is distributed as $x_j \sim N(m_0, \sigma_0)$ and the values $n_d = 10^6$ and $n_b = 10^3$ were used in construction of the ensemble and histogram. In the short-term regime, $n \leq 3$ in this example, the histogram remains approximately normal and the most likely value for x is accurately described by images of the measured value $f^{(n)}(m_0, a)$. We also note the standard deviation increases with time, $\sigma_{n+1} \approx |f'(f^{(n)}(m_0, a), a)|\sigma_n$, reflecting a growth in the uncertainty of the most likely value. At $n = 3$ there is a significant probability the measured value will be near the critical point (a quantitative test will be introduced below). A new peak in the histogram is created at the image of the critical point $f(x_c, a)$, at the next time step. For time $4 \leq n \leq 7$, following this new peak accurately describes the most likely trajectory.

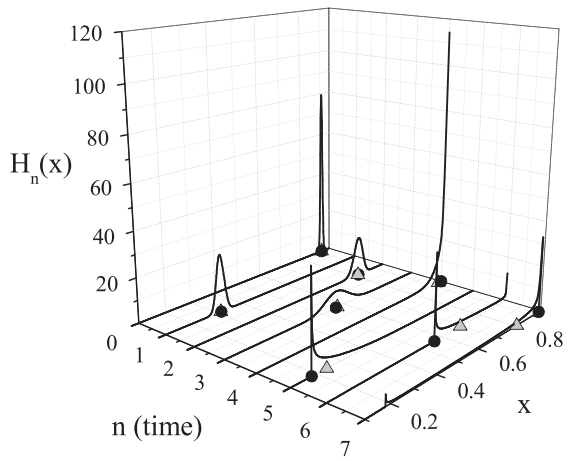

FIG. 1. An example of evolution of an initial condition with uncertainty. The underlying map dynamics are governed by the Logistic map at $a = 3.80$, resulting in chaotic dynamics. At each time step a histogram is shown along with the trajectory of the initial measurement $f^{(n)}(m_0, a)$ (gray triangle), and the most likely trajectory (black circle). At time $n = 7$ the error in prediction produced by following $f^{(n)}(m_0, a)$ is approximately 20% of the attractor size.

The origin of the new peak can be understood by introducing the Frobenius-Perron operator, which describes the time evolution of a probability density driven by map dynamics. For noise-free map dynamics, as described in Eq. (1), the operator can be written

$$\rho_{n+1}(x) = \sum_j \frac{\rho_n(f_j^{(-1)}(x, a))}{|f'(f_j^{(-1)}(x, a), a)|}. \tag{4}$$

The sum is over all inverses j of the map given by $x_n = f_j^{(-1)}(x_{n+1}, a)$. The requirements for Eq. (1) have clear implications for the resulting evolution of the probability density. The denominator in Eq. (4) can be equal to zero. If the probability density overlaps a critical point at time n a singularity will be created at time $n + 1$. This is the origin of the new peak in Fig. 1. As discussed in [18], the ill-behaved singularity in an exact mathematical treatment appears as a smoothed peak in a histogram which reflects measurement with finite resolution.

The key to extending prediction is to recognize cases when the probability density near the critical point(s) is sufficient to create a new peak. For this purpose, we define a ratio

$$\mathcal{R}_n^i = \frac{\int_{x \in n(f(x_c^i, a))} dx \rho_{n+1}(x)}{\int_{x \in n(f(\mu_n, a))} dx \rho_{n+1}(x)}. \tag{5}$$

This ratio compares the probability associated with a small region near the image of the critical point, which we label $n(f(x_c^i, a))$, to the probability in a small region near the image of the current most probable state $n(f(\mu_n, a))$.

Motivated by the observations in Fig. 1 and knowledge of the probability density dynamics given in Eq. (4), we propose the approximation $\rho_n(x) \approx N(x; \mu_n, \sigma_n)$. This is not meant to be an accurate representation of the true probability density. Rather, this approximation serves as a tool for recognition of folds which will create new peaks. In this spirit, the dynamics of the most likely point μ_n, and standard deviation of the density σ_n, are given by

$$\mu_{n+1} = \begin{cases} f(\mu_n, a) & \mathcal{R}_n^i < 1 \\ f(x_c^i, a) & \mathcal{R}_n^i \geq 1, \end{cases} \tag{6a}$$

$$\sigma_{n+1} = |f'(\mu_n, a)|\sigma_n. \tag{6b}$$

We set the initial values to reflect the measurement with uncertainty, $\mu_0 = m_0$ and σ_0^2 reflecting the variance in $\rho(r)$. We expect that this approximation is only effective in the short- and medium-term regimes, reflected by a

small value for σ_n. In practice, the presence of many pronounced peaks in the histogram reflects the end of meaningful trajectory prediction.

For application of Eq. (6), a reasonable approximation for $\mathcal{R}_n^i$ must be found. We consider a linear expansion of Eq. (1) about the current most likely point, $f(x, a) = f(\mu_n, a) + (x - \mu_n)f'(\mu_n, a) + \mathcal{O}((x - \mu_n)^2)$. The probability in the region $n(f(\mu_n, a)) = [f(\mu_n, a) - \Delta x/2, f(\mu_n, a) + \Delta x/2]$ can be found by assuming uniform density at the preimage of the region of interest $f^{(-1)}[n(f(\mu_n, a)), a]$, and invoking conservation of probability. Under these assumptions, we find the denominator of Eq. (5) is approximately $(\rho_n(\mu_n)\Delta x)/|f'(\mu_n, a)|$.

Near one of the critical points, a quadratic expansion of Eq. (1) must be used, $f(x, a) = f(x_c^i, a) + 1/2(x - x_c^i)^2 f''(x_c^i, a) + \mathcal{O}((x - x_c^i)^3)$. Next, we consider the probability associated with the neighborhood $n(f(x_c^i, a))$. If x_c^i is a local maxima, this region is $n(f(x_c^i, a)) = [f(x_c^i, a) - \Delta x, f(x_c^i, a)]$. Making the same approximations as above, we find the numerator in Eq. (5) is approximately $2\sqrt{(2\Delta x)/|f''(x_c^i, a)|}\rho_n(x_c^i)$. Combining these results, we obtain

$$\mathcal{R}_n^i \approx 2|f'(\mu_n, a)|\sqrt{\frac{2}{\Delta x|f''(\mu_n, a)|}}\frac{\rho_n(x_c^i)}{\rho_n(\mu_n)}. \quad (7)$$

In application of this result, Δx should be set equal to measurement resolution in experiment and bin size in ensemble simulation. We also employ the approximation discussed above, $\rho_n(x) \approx N(x; \mu_n, \sigma_n)$.

One hundred ensemble simulations were performed to test the effectiveness of Eqs. (6) and (7) using the Logistic map. For each simulation a uniform random value on the unit interval was generated, $x_r = \text{rand}[0, 1]$. Next, the map was applied for 500 time steps to ensure a typical value on the attractor and the measured value set, $m_0 = f^{(500)}(x_r, a)$. Finally, a set of $n_d = 2 \times 10^6$ initial conditions was generated using a normal distribution, $x_j \sim N(m_0, \sigma_0)$, where $\sigma_0 = 5 \times 10^{-3}$.

At each time step the most likely trajectory, corresponding to the bin with the largest probability density as given in Eq. (3), is obtained and given the value $h_n = x_i$. For our purposes, the value of h_n is considered to be the true most likely trajectory. Two methods of predicting this value are considered. We track the image of the initial most likely point $f^{(n)}(m_0, a)$, and the results of our method μ_n as given in Eq. (6a).

We define two values which provide a numerical measure of the prediction *accuracy*

$$A_{i,n} = -\log_{10}|f^{(n)}(m_0, a) - h_n| \quad (8a)$$

$$A_{m,n} = -\log_{10}|\mu_n - h_n|. \quad (8b)$$

$A_{i,n}$ describes the accuracy obtained by iterating the measured value with a perfect model and $A_{m,n}$ the accuracy from application of Eq. (6). In this form, these values reflect the number of decimal places of accuracy for each approach. As a result, larger values reflect a more accurate prediction.

Figure 2(a) provides the results of 100 simulations of the Logistic map at $a = 3.80$. Only data for post spike time, which starts when the first fold occurs in each simulation, are provided. Before the first fold (not shown), the predictions for $f^{(n)}(m_0, a)$ and μ_n are exactly the same. A value near 4 for either $A_{i,n}$ or $A_{m,n}$ demonstrates prediction accuracy representative of the histogram resolution. For each prediction method, the median accuracy and bars which show the (10th, 90th) percentiles are provided. The results demonstrate increased prediction accuracy for the proposed method, $A_{m,n} \geq A_{i,n}$, for three time steps in 87 of 100 trials conducted.

In Fig. 2(b), we consider the presence of dynamical noise by modifying Eq. (1) to read $x_{n+1} = f(x_n, a) + \xi_n$, where $\xi_n \sim N(0, \sigma)$. As in Fig. 2(a), we consider the Logistic map at $a = 3.80$. Although this method was not expressly designed to handle dynamical noise, the results of 100 simulations at each value of σ demonstrate increased prediction accuracy. Only when 6σ is approximately 13% of the attractor size does the proposed method not provide a benefit.

Finally, we consider application of these ideas to prediction of higher dimensional maps and ordinary differential equations. Maps will have fold dynamics when the determinant of their Jacobian can be equal to zero. Weakly coupled Logistic maps, which have multiple positive Lyapunov exponents, is a convenient example. Each of the coupled maps can fold independently or simultaneously. For effective application of this method, all possible combinations of folds should be found and a set of ratios similar to Eq. (5) derived. Although more complex,

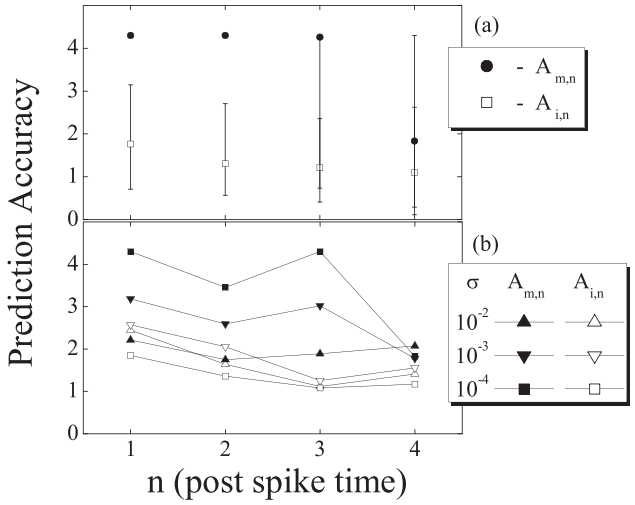

FIG. 2. Prediction accuracy of the proposed algorithm. Post spike time $n = 1$ corresponds to the first fold in the probability density. (a) Data provided show the results for prediction without noise. The median accuracy with bars which indicate the (10th, 90th) percentiles are provided. (b) Median prediction accuracy is provided for various levels of dynamical noise.

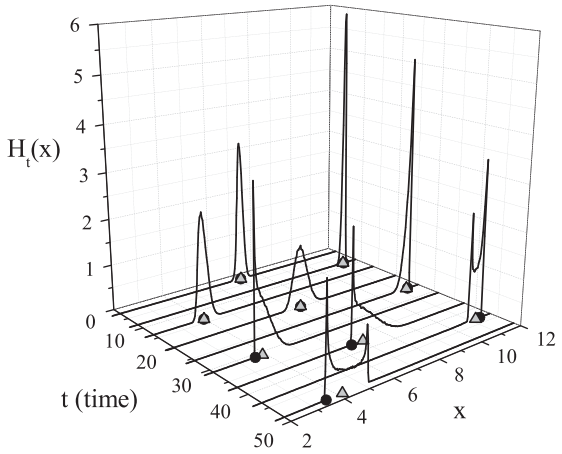

FIG. 3. An example of folding of the probability density in the Rössler attractor. Each time x reaches a local maximum in its dynamics a histogram of the ensemble is shown. The most likely trajectory (black circle) and the path of the initial measurement (gray triangle) are also provided.

no fundamentally new ideas are needed to understand this example.

For application to ordinary differential equations we consider the return map generated by the sequence of maxima from one of the variables, often called the *Lorentz* map. As an example we introduce the Rössler attractor, given by the equations $dx/dt = -y - z$, $dy/dt = x + ay$, and $dz/dt = b + (x - c)z$. If we consider the sequence of maxima in the x dynamics, we find the return map approximates the unimodal properties required of Eq. (1) and we expect to observe folding.

In Fig. 3 we see the evolution of an ensemble of 50 000 trajectories obtained by 4th order Runge-Kutta with values $a = 0.2$, $b = 0.2$, and $c = 5.7$. Each time the x dynamics reaches a maxima, a histogram is created from the ensemble. Folding dynamics are clearly present and we note the most likely trajectory and the evolution of the initial measured value do not agree beyond the short term. We expect application of the methods we have introduced to extend prediction in this case as well.

In this Letter we have demonstrated that knowledge of ensemble dynamics can be used to extend prediction when there is uncertainty in measurement of the initial condition. A fold can be detected and the predicted trajectory adjusted appropriately. Application to the Logistic map demonstrates the effectiveness of this method and preliminary results using the Rössler attractor demonstrate the potential for application of these ideas to ordinary differential equations.

The authors wish to acknowledge insightful discussions and helpful suggestions in preparing this manuscript from Joseph Jun and Glenn Foster. This work was supported by National Science Foundation Grants No. NSF PHY 01-40179, No. NSF DMS 03-25939 ITR, and No. NSF DGE 03-38215.

[1] N. Gershenfeld, B. Schoner, and E. Metois, Nature (London) **397**, 329 (1999).
[2] V. F. Pisarenko and D. Sornette, Phys. Rev. E **69**, 036122 (2004).
[3] P. E. McSharry and L. A. Smith, Phys. Rev. Lett. **83**, 4285 (1999).
[4] K. Lehnertz and C. E. Elger, Phys. Rev. Lett. **80**, 5019 (1998).
[5] O. N. Bjørnstad and B. T. Grenfell, Science **293**, 638 (2001).
[6] L. M. Hively and V. A. Protopopescu, Chaos **14**, 408 (2004).
[7] J. Harlim, M. Oczkowski, J. A. Yorke, E. Kalnay, and B. R. Hunt, Phys. Rev. Lett. **94**, 228501 (2005).
[8] L. A. Smith, Proc. Natl. Acad. Sci. U.S.A. **99**, 2487 (2002).
[9] H. D. I. Abarbanel *et al.*, Rev. Mod. Phys. **65**, 1331 (1993).
[10] J. L. Breeden and A. Hübler, Phys. Rev. A **42**, 5817 (1990).
[11] J. D. Farmer and J. J. Sidorowich, Phys. Rev. Lett. **59**, 845 (1987).
[12] P. Cvitanović, Phys. Rev. Lett. **61**, 2729 (1988).
[13] S. Grossmann and S. Thomae, Z. Naturforsch. A **32**, 1353 (1977).
[14] R. F. Fox, Chaos **5**, 619 (1995).
[15] A. Lasota and M. C. Mackey, *Chaos, Fractals, and Noise* (Spring-Verlag, New York, 1994), 2nd ed.
[16] R. May, Nature (London) **261**, 459 (1976).
[17] O. E. Rössler, Phys. Lett. A **57**, 397 (1976).
[18] R. Shaw, Z. Naturforsch. A **36**, 80 (1981).